Complex magnetic phase diagram of a geometrically frustrated Sm lattice: Magnetometry and neutron diffraction study of $SmPd_2Al_3$

J. Pospíšil,[1] G. Nénert,[2] S. Miyashita,[3] H. Kitazawa,[4] Y. Skourski,[5] M. Diviš,[1] J. Prokleška,[1] and V. Sechovský[1]

[1]*Faculty of Mathematics and Physics, Department of Condensed Matter Physics, Charles University, Ke Karlovu 5, 121 16 Prague 2, Czech Republic*

[2]*Institut Laue Langevin, BP 156, 6 rue Jules Horowitz, 38042, Grenoble Cedex 9, France*

[3]*Department of Physics, School of Science, The University of Tokyo 7-3-1 Hongo, Bunkyo-ku, Tokyo, 113-0033 Japan*

[4]*National Institute for Materials Science, Tsukuba, Ibaraki 305-0047, Japan*

[5]*Dresden High Magnetic Field Laboratory, Helmholtz-Zentrum Dresden Rossendorf, D-01314 Dresden, Germany*

(Received 6 March 2013; published 5 June 2013)

Magnetism in $SmPd_2Al_3$ was investigated on a single crystal by magnetometry and neutron diffraction. $SmPd_2Al_3$ represents a distinctive example of a Sm magnetism exhibiting complex magnetic behavior at low temperatures with four consecutive magnetic phase transitions at 3.4, 3.9, 4.4, and 12.5 K. The rich magnetic phase diagram of this compound reflects the specific features of the Sm^{3+} ion, namely, the energy nearness of the ground-state multiplet $J = 5/2$ and the first excited multiplet $J = 7/2$ in conjunction with strong crystal field influence. Consequently, a significantly reduced Sm magnetic moment in comparison with the theoretical Sm^{3+} free-ion value is observed. Despite the strong neutron absorption by natural samarium and the small Sm magnetic moment ($\sim 0.2\ \mu_B$), we have successfully determined the magnetic **k** vector (1/3, 1/3, 0) of the phase existing in the temperature interval 12.5–4.4 K. This observation classifies the $SmPd_2Al_3$ compound as a magnetically frustrated system. The complex magnetic behavior of this material is further illustrated by kinetic effects of the magnetization, inducing a rather complicated magnetic structure with various metastable states.

DOI: 10.1103/PhysRevB.87.214405 PACS number(s): 75.10.Dg, 75.30.Gw

I. INTRODUCTION

The $SmPd_2Al_3$ compound belongs to the class of rare-earth (R) materials crystallizing in the hexagonal crystal structure of the $PrNi_2Al_3$-type (space group $P6/mmm$).[1] The physical properties of the R counterparts with the composition RPd_2Al_3 (for R = Ce, Pr, Nd Sm, and Gd) are controlled mainly by the strong influence of the crystal field (CF) on the magnetic state of the R ions.[1,2] This leads to various types of magnetic order (for R = Ce, Nd, Sm, and Gd)[3–7] or contrary paramagnetic ground state (Pr).[8] $CePd_2Al_3$ has been reported as a heavy fermion antiferromagnet.[9] Finally, the Y and La compounds are superconductors.[10–12] The RPd_2Al_3 compounds provide an interesting playground for theoreticians. They are model examples for studying R magnetism due to their high variability of the physical properties connected with a simple and high-symmetry crystal structure.[10,13–15] Although physical properties of all compounds in the RPd_2Al_3 series were subjected to intensive research activities, the two most interesting cases—Gd and Sm compounds—remain poorly understood despite the recent progress within last years.[13,16]

$SmPd_2Al_3$ was described as an antiferromagnet with strong uniaxial anisotropy even in the paramagnetic state with the easy-magnetization direction along the crystallographic c axis. Four successive magnetic transitions have been identified in the temperature dependence of specific heat at temperatures $T_3 = 3.4$ K, $T_2 = 3.9$ K, $T_1 = 4.3$ K, and $T_C = 12.5$ K. The high number of the magnetic phase transitions and the series of four magnetic field induced transitions detected at 0.03, 0.35, 0.5, and 0.75 T, respectively, at 1.8 K yield a complex magnetic phase diagram.

Generally, the complexity of the Sm magnetism is intimately connected with the anomalous magnetic ground state of the Sm^{3+} ion.[17] The Sm^{3+} ground-state multiplet $J = 5/2$ is radically influenced by the near first and second excited multiplets $J = 7/2$ and $J = 9/2$ that are lying above only 129.3 and 277.9 meV, respectively.[17] As a consequence, distinctive features like multiple magnetic phase transitions and the susceptibility influenced via the temperature-independent Van Vleck term are observed.[18]

Neutron scattering is usually a good tool to study magnetism on a microscopic scale. However, Sm-containing materials are usually disregarded due to high thermal-neutron absorption by natural samarium. In addition, another difficulty arises from the usually low magnetic moment of the Sm^{3+} ion. The natural Sm consists of seven isotopes.[19,20] The high thermal-neutron absorption of the natural samarium (^{nat}Sm) is given mainly by isotopes ^{149}Sm, ^{150}Sm, and ^{152}Sm with total average absorption of the ^{nat}Sm 5922 b.[21–23] There are two ways offered for overcoming the high neutron absorption problem. The first one is to work with isotopic samarium, typically ^{154}Sm, which combines low neutron absorption and high coherent scattering length. Unfortunately, the cost of ^{154}Sm isotope (99%) metal is too high to buy enough material for guaranteed single-crystal growth for such an experiment. The second choice is to use the fact that the magnitude of the neutron absorption strongly depends on neutron energy.[24] Consequently, higher energy neutrons ("hot" neutrons[25,26]) are a good alternative. Therefore, we have carried out a single-crystal neutron diffraction experiment using the D9 high-resolution diffractometer at the hot source in the Institut Laue Langevin (ILL), Grenoble, France.

In this paper, we have constructed a detailed magnetic phase diagram of $SmPd_2Al_3$ using detailed magnetization data and investigated the nature of the first magnetic phase

using the single-crystal neutron diffraction on natural isotopic $SmPd_2Al_3$.

II. EXPERIMENTAL AND COMPUTATIONAL DETAILS

The single crystal of the $SmPd_2Al_3$ compound has been grown in a triarc furnace by the Czochralski pulling method from stoichiometric amounts of elements. Pulling and single crystal growth details and quality were already described in Ref. 13. The natural isotope of Sm has been used.

The samples of the appropriate shape for the magnetization and neutron experiment, respectively, have been cut by a wire saw (South Bay Technology Inc., type 810). The sample for the magnetization measurements had the dimensions $1 \times 1 \times 1.5$ mm^3 with rectangular planes oriented perpendicularly to the crystallographic axes a and c. A single crystal of the size $1.9 \times 1.8 \times 2.2$ mm^3 was used for the neutron diffraction experiment. All planes of the samples were polished and cleaned using successively the 6, 3, and 1-μm diamond particle suspension. The orientation of each as-prepared sample was checked by the backscattering Laue technique using the Cu white x-ray radiation before measurements.

The magnetization measurements were performed using a commercial Quantum Design Magnetic Property Measurement System device. The high-field magnetization experiment was carried out with the extraction method using the 40-T class hybrid magnet in the High Magnetic Field Laboratories of the National Institute for Materials Sciences in Tsukuba, Japan. The pulse magnetic field experiment was realized in 60-T magnet in the Dresden High Magnetic Field Laboratory in Germany. The theoretical magnetic isotherms were calculated within the crystal field model introduced in our previous work.[13]

Single-crystal neutron diffraction data were collected on the high resolution four-circle diffractometer D9 at the ILL, Grenoble, using the wavelength of 0.5109(1) Å obtained by reflection from a Cu (220) monochromator. The wavelength was calibrated using a germanium single crystal. D9 is equipped with a small two-dimensional (2D) area detector,[27] which for this measurement allowed optimal delineation of the peak from the background. FullProf was used for the refinement of the crystal structure at 20 K. The absorption correction was carried out using the shape of the crystal and its indexed faces to obtain the geometrical factor. The absorption correction was calculated using the absorption cross sections. For all data, background corrections following Wilkinson and Lorentz corrections were applied.[28]

III. CRYSTAL STRUCTURE ANALYSIS

The crystal structure refinement at 20 K was based on the single-crystal neutron diffraction data collection of the 149 unique reflections. The best data fit with $R(F^2) = 6.14\%$ is presented in Fig. 1. We have confirmed that $SmPd_2Al_3$ at 20 K crystallizes in the space group $P6/mmm$ with the cell parameters $a = b = 5.3970(4)$ Å and $c = 4.1987(5)$ Å. These values compare well to the previously published cell parameters.[1,7] The corresponding atomic coordinates that are all in the special Wyckoff positions and the anisotropic displacement parameters are given in Table I. No crystal structure phase transition has been observed from room temperature down to 2 K.

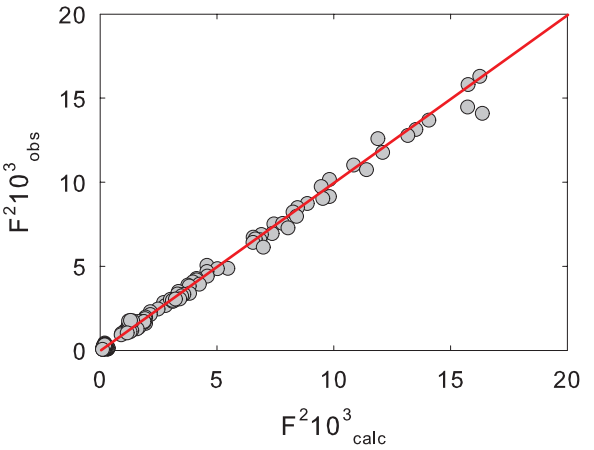

FIG. 1. (Color online) Calculated versus observed values of the squared intensities for data collected at 20 K.

IV. MAGNETIC PHASE DIAGRAM STUDY

First, we have studied magnetization curves at low temperature $T = 1.7$ K and magnetic field up to 30 T using a hybrid magnet (at Tsukuba High Magnetic Field Laboratory) with the field applied along the crystallographic axes a and c and the in-plane (210) direction. We have found clear evidence of the easy-axis type anisotropy with axis c as the direction of easy magnetization (see Fig. 2). If one assumes the constant slope of the magnetization curve for each axis without any metamagnetic transition, the magnetization along the hard axis in the basal plane will attain to the magnetization along the c axis at 79.8 T.

The behavior of the magnetization curves clearly denotes a strong easy-axis-type magnetic anisotropy. A small discrepancy of magnetization curves for the hybrid magnet and the SQUID magnetometer along the c axis (discussed later) may come from the difference of temperatures of measurements and/or a wrong estimation of the background.

Before exploring the temperature and magnetic field dependence of the phase diagram in more details, we have focused on

TABLE I. Atomic coordinates and anisotropic displacement parameters as determined at temperature 20 K.

	X	Y	Z	U_{11} (Å^2)	U_{22} (Å^2)	U_{33} (Å^2)	U_{12} (Å^2)	U_{13} (Å^2)	U_{23} (Å^2)
Al	1/2	0	1/2	0.0028(7)	0.0021(7)	0.0028(9)	0.0011(7)	0	0
Pd	1/3	2/3	0	0.0012(6)	0.0012(6)	0.0007(6)	0.0006(6)	0	0
Sm	0	0	0	0.0081(8)	0.0081(8)	0.0084(11)	0.0040(8)	0	0

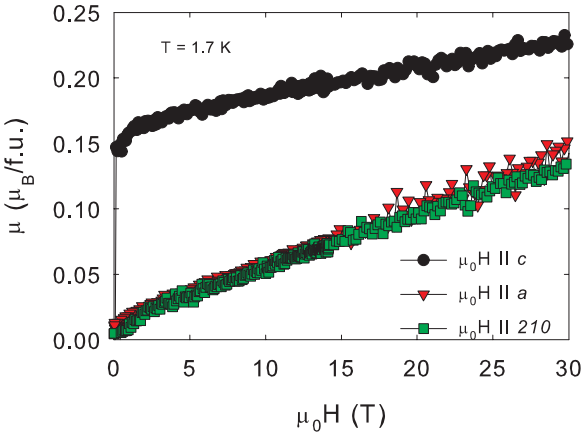

FIG. 2. (Color online) Magnetization curves measured at 1.7 K with magnetic field applied along the axes a and c, respectively, and also along the in-plane (210) direction.

the magnetic behavior of the $SmPd_2Al_3$ compound published in previous works. Precise magnetization loops were measured exhibiting complex magnetic features with a complicated steplike shape.[6,13] The heat capacity data published in Ref. 13 shows four successive magnetic transitions at $T_3 = 3.4$ K, $T_2 = 3.9$ K, $T_1 = 4.4$ K, and $T_C = 12.5$ K in the zero magnetic field. We may regard the system as a spin $S = 1/2$ system from the published crystal field analysis. The energy gap to the next spin doublet is about 100 K, and it would not affect low-temperature properties below 12 K. The spin degree of freedom exhibits magnetic phase transitions (see Ref. 13). Finally, the expected magnetic phase diagram of the $SmPd_2Al_3$ is complicated not only due to the four successive magnetic transitions observed in the specific-heat data in zero magnetic field but furthermore by a series of field-induced magnetic phase transitions (see Refs. 6 and 13).

Considering the heat capacity data (Ref. 13), we have investigated the temperature evolution of the magnetization loops in the temperature range 1.8–5 K by 0.1 K steps. The magnetic field was applied along the c axis, which is the easy-magnetization axis. Another four magnetization loops have been measured also in the temperature range 5–12 K. The magnetization loops can be found in Figs. 3–5. These results allowed us drawing of the magnetic phase diagram of $SmPd_2Al_3$, which will be shown in Fig. 6.

Figure 3(a), contains three representative loops for the interval from 1.8 to 2.9 K, which covers the region below T_3. Three magnetic field-induced transitions can be identified on the magnetization curves within this interval. In Figs. 3(b) and 3(c), we present a zoom into the magnetic field regions where the phase transitions occur. At 1.8 K, the onset of the first transition (below which the zero-field-cooled phase labeled $P1$ exists) is located at $\mu_0 H_{C1} = 0.038$ T. The second field-induced transition is spread over the interval from 0.35 T and 0.55 T ($\mu_0 H_{C2}$). The latter field is considered as a point for construction of the magnetic phase diagram. The phase existing between the first and second transition is labeled $P2$. The third transition is broad extending up to $\mu_0 H_{C3} = 2.5$ T. This is taken as the characteristic field of the third transition in the magnetic phase diagram. The

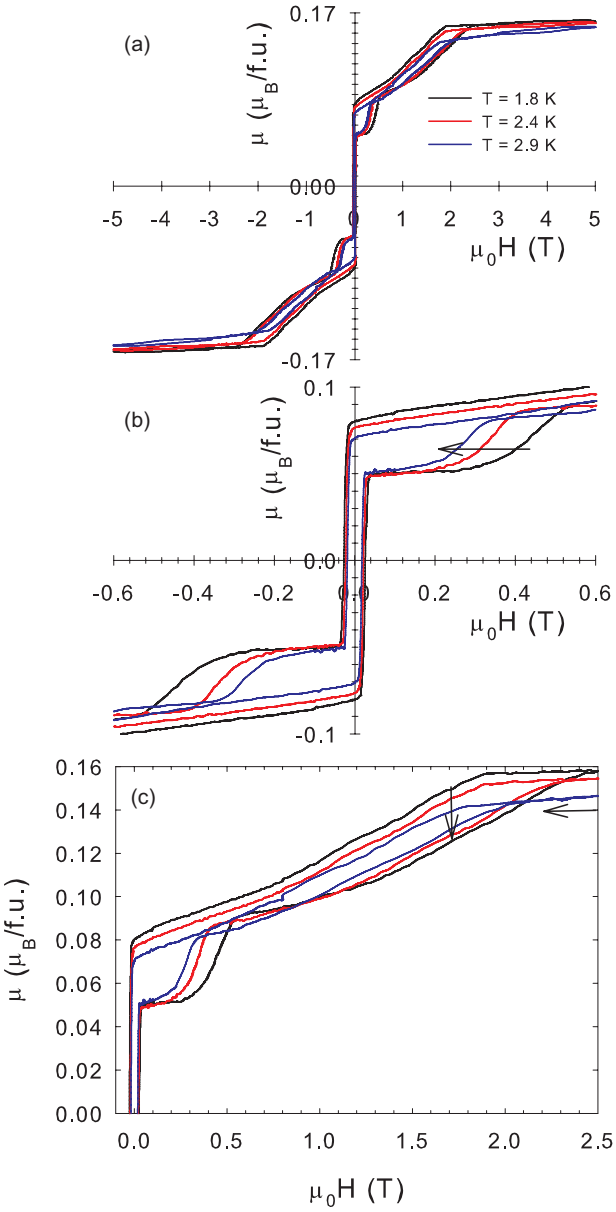

FIG. 3. (Color online) (a) Magnetization loops measured in the temperature interval 1.8–2.9 K. Only three representative loops are displayed. (b) Low-magnetic field features of the loops. Gradual vanishing of the hysteresis and shifts of the steps in the loops to lower magnetic fields with increasing temperature is indicated by arrows. (c) Magnetic field loops in the positive field quadrant up to the saturation field.

phase existing between the second and third transition is labeled $P3$. Above $\mu_0 H_{C3} = 2.5$ T, a stable high magnetic field phase $P4$ survives at least up to 60 T, which was the highest measured magnetic field in our work. The branches of the loops recorded in the magnetic field decreasing from 5 to 0 T demonstrate the hysteresis of the field-induced transitions. The first drop of the magnetization has been found commencing at $\mu_0 H_{C4} = 1.9$ T, i.e., the third transition has a hysteresis of 0.6 T (=2.5–1.9 T) as will be shown in Fig. 6. The first drop of magnetization is followed by continuous decrease of the magnetic moment, which ends in

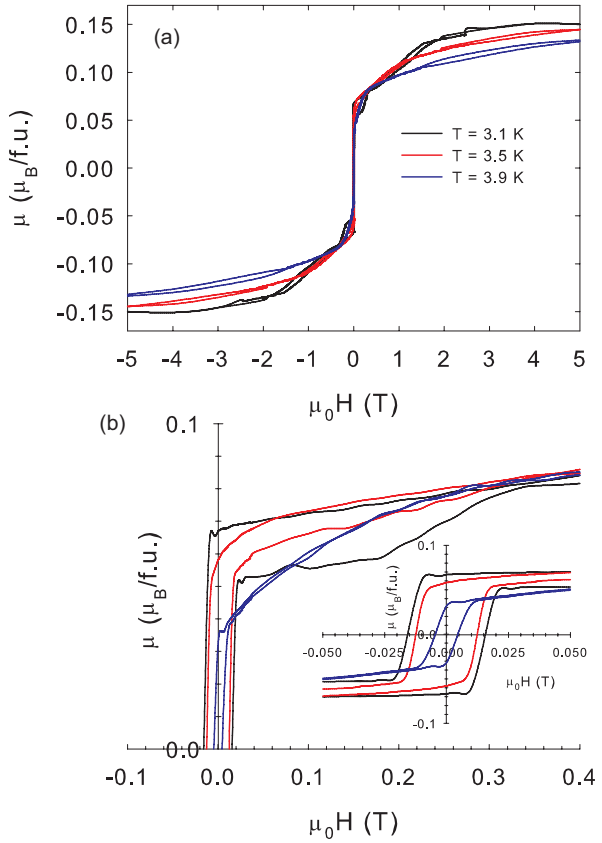

FIG. 4. (Color online) (a) Representative magnetization loops measured in the temperature interval between 3.1–3.9 K. (b) Low magnetic field features of the loops, namely, the gradual reduction of hysteresis and shifts of steps in the loops to lower fields. Dramatic changes occur in this temperature interval when hysteresis disappears at ∼3.5 K and also the $P2$ phase disappears between 3.7–3.9 K.

the magnetic field of -0.038 T by magnetization reversal. The further increase of the negative magnetic field (from 0 to -5 T) after magnetization reversal leads to symmetric magnetization processes and transitions with respect the quadrant with positive magnetic field. It also indicates a symmetric phase diagram in the positive and negative magnetic field, respectively. When increasing temperature, the hysteresis of both transitions becomes gradually reduced, and the fields of the three transitions simultaneously decrease as it is marked by arrows in Fig. 3(b) and 3(c).

Figures 4(a) and 4(b) show the temperature evolution of the hysteresis loops in the temperature interval 3.1–3.9 K. The first significant change of the loops is expected in this interval because two magnetic phase transitions in zero field were predicted at temperatures 3.4 and 3.9 K from specific-heat data.[13] All of the three field-induced transitions described in Fig. 3 are conserved up to 3.4 K; nevertheless, a dramatic suppression of the second transition originally occurring in the field interval 0.35 T–0.55 T is evident. It is accompanied by a fast reduction of hysteresis, which vanishes at ∼3.5 K. The second dramatic change is the merging of the phases $P2$ and $P3$ at ∼3.8 K. The resulting new phase is called $P5$. Above ∼3.8 K, only the $P1$ phase and the common weak knee of the new phase $P5$ appearing around 0.2 T–0.3 T remain (Fig. 4).

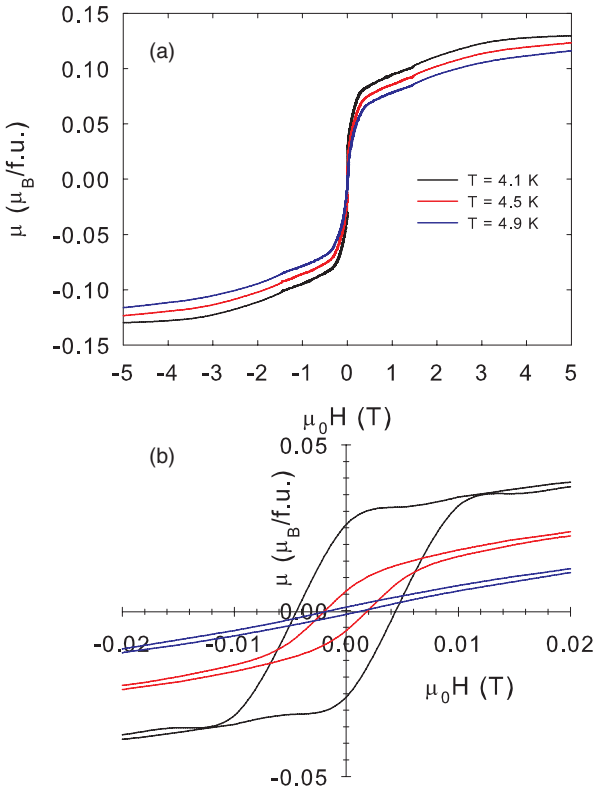

FIG. 5. (Color online) (a) Group of magnetization loops measured in temperature interval between 4.1–4.9 K. (b) Low magnetic field features of loops. Gradual vanishing of the $P1$ phase is evident.

The third set of loops in Figs. 5(a) and 5(b) was collected in between 4.1 and 4.9 K. The temperature interval 3.8–4.5 K is characterized by the coexistence of the $P1$ phase and the $P5$ phase. The $P1$ phase simultaneously disappears at a temperature of ∼4.5 K [Fig. 5(b)]. Above 4.5 K, only the $P5$ phase survives as a weak knee up to ∼12 K, where the magnetization becomes weak and linearly changing with the field.

V. MAGNETIC STRUCTURES STUDY

Based on the magnetization data, we have sketched the complex magnetic phase diagram of $SmPd_2Al_3$, as shown in Fig. 6. However, the nature of the various magnetic phases

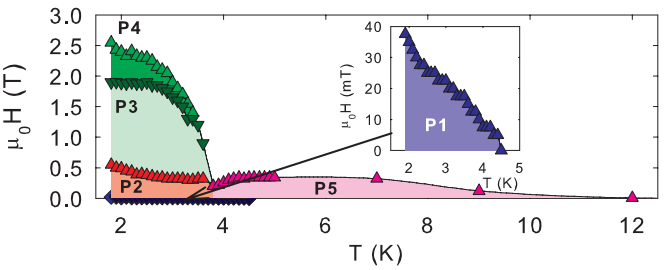

FIG. 6. (Color online) Magnetic phase diagram of $SmPd_2Al_3$ compound constructed on the basis of magnetization data in the magnetic field applied along the c axis. The triangles pointing up (down) represent the transition for magnetic field sweeping up (down). The difference between the two points for constant temperature represents the hysteresis of the transition.

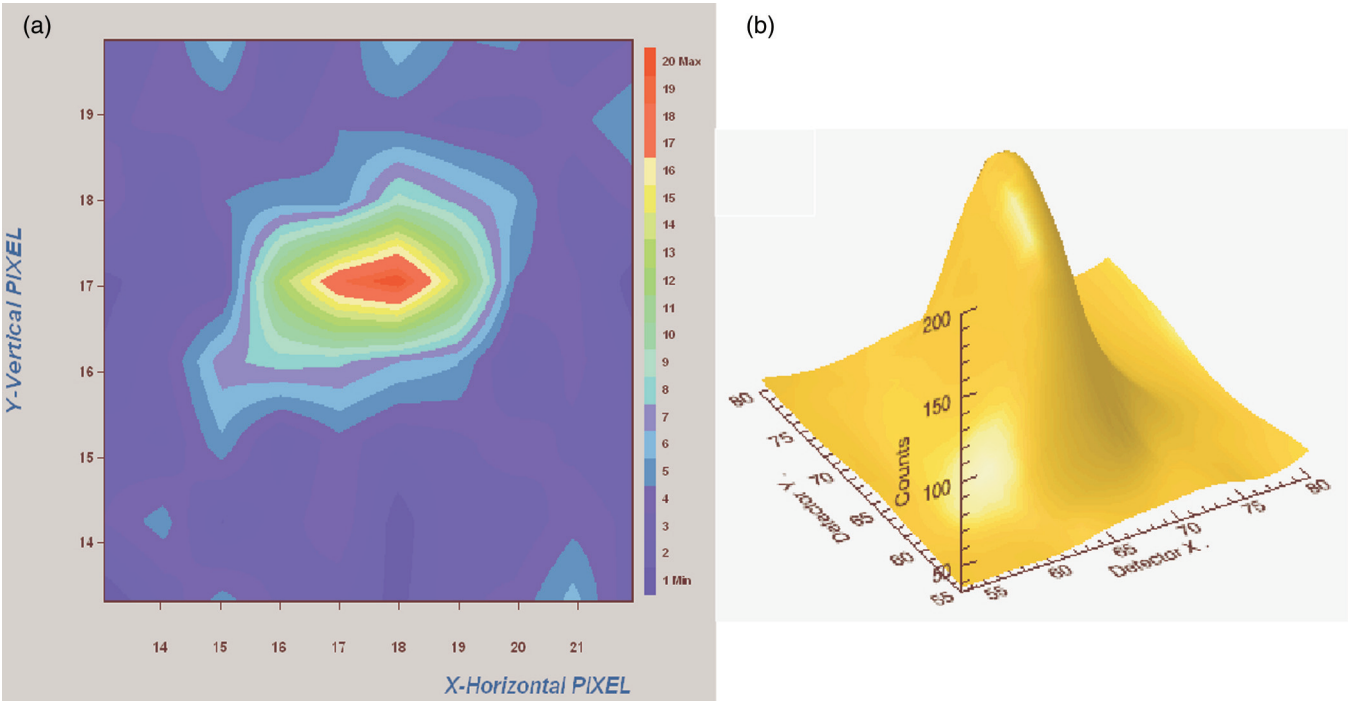

FIG. 7. (Color online) Reflection (5/3, 5/3, 0) as observed at 3.6 K. (a) Filled contour plot showing the reflection as recorded in the 2D detector. (b) 3D plot of the reflection.

remained unknown. Consequently, we have carried out single-crystal-neutron diffraction experiment using the D9 four-cycle diffractometer with a short wavelength $\lambda = 0.511$ Å. We have cooled down the crystal below T_C and carried out q scans. Despite the weak magnetic moment (the saturated magnetic moment is only 0.16 μ_B/f.u.) and the strong absorption, we were able to observe magnetic reflections. One of the strongest magnetic reflections (5/3, 5/3, 0) is illustrated in Fig. 7. The Miller indices of the magnetic reflections are of the type (h, k, 0) in good agreement with magnetization data evidencing the easy magnetization axis along the c axis; the **k** vector of the ground-state magnetic structure has been determined as **k** = (1/3, 1/3, 0) and the symmetry conditions given by the $P6/mmm$ space group. No component of the magnetic moment has been detected in other crystallographic directions by magnetization measurements.

Due to the weakness of the magnetic reflections resulting from the high absorption of natural samarium and low magnetic moment, we could not carry out omega scans but only acquisition at the top of the reflections. Consequently, we do not have meaningful integrated intensities of the available magnetic reflections (contrary to the nuclear reflections), and therefore we cannot derive the value of the magnetic moment from the single-crystal neutron diffraction data. We could acquire only the intensity at the top of a restricted number of magnetic reflections using the 2D area detector and followed few reflections as functions of temperature. Figure 8 presents the temperature dependence of the (5/3, 5/3, 0) reflection that appeared to be the strongest.

We can clearly see that the magnetic reflection (5/3, 5/3, 0) emerges at about 12.4 K, which corresponds well to the T_C determined from specific-heat measurements.[4–7,13] Further decrease of temperature leads to an increase of the (5/3, 5/3, 0) reflection intensity with a maximum around 4.5–5 K, which corresponds quite well to T_1.[13] The intensity of the (5/3, 5/3, 0) reflection suddenly drops with further decreasing temperature. This corresponds to the critical temperature T_2 (3.9 K),[13] where the propagation vector probably changes. The extremely weak magnetic signal and the lack of resolution in q due to the short neutron wavelength prevented confirmation of this hypothesis.

The expected anomalies at T_1 and T_3 are not so clearly visible. The presence of the last anomaly T_3 at 3.4 K is an open question when taking into account the error bars of the intensity.

VI. DISCUSSION

Below T_C, the intensity of the reflection (5/3, 5/3, 0) behaves as an order parameter that could be fitted to a power law as $I = a * (T_C - T)^{\beta}$. The resulting fit is presented in Fig. 9. The obtained critical exponent is close to 0.5, suggesting that the behavior of $SmPd_2Al_3$ between T_C and T_1 can be described within the mean-field theory.

In addition, we have inspected several other measured magnetic reflections such as (4/3, 1/3, 0), (1/3, 4/3, 0), (1/3, 1/3, 0), and (2/3, 2/3, 0). No magnetic reflection with $l \neq 0$ has been detected. This observation is consistent with the magnetic ordering of Sm magnetic moments parallel to the c axis, which means a collinear magnetic structure. On the other hand, we are aware that magnetic reflections due to a possible slight off c axis component may not be detectable within our experiment, and therefore we can take the scenario with the Sm magnetic moments parallel to the c axis only tentatively. Taking into account that the propagation vector between T_C and T_1 is **k** = (1/3, 1/3, 0) and *a priori* no magnetic component is in the basal plane, we can give a representation of this likely magnetic structure (see Fig. 10). The magnetic unit cell is

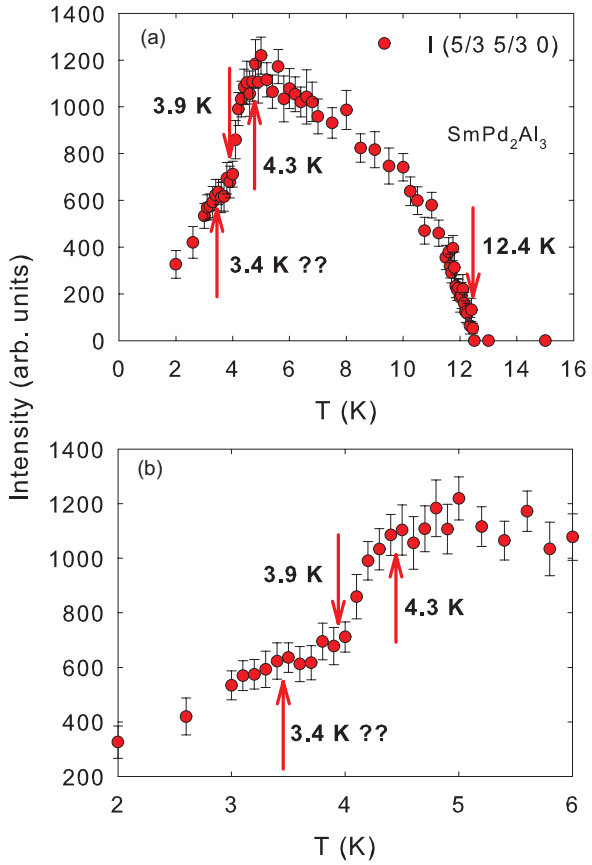

FIG. 8. (Color online) Temperature dependence of the (5/3, 5/3, 0) reflection. (a) The temperature evolution in the whole temperature range. (b) Zoom in the temperature range 2 to 6 K. The red arrows mark the transition temperatures as determined from specific heat. The presence of the last transition at temperature $T_3 = 3.4$ K is disputable within the error bars.

three times larger along a and b, respectively, and is formed by two hexagonal sublattices that are interpenetrated and are coupled antiferromagnetically. The coupling along the c axis is ferromagnetic.

The magnetic structure between T_C and T_1 characterized by $\mathbf{k} = (1/3, 1/3, 0)$ with a hexagonal lattice can be discussed

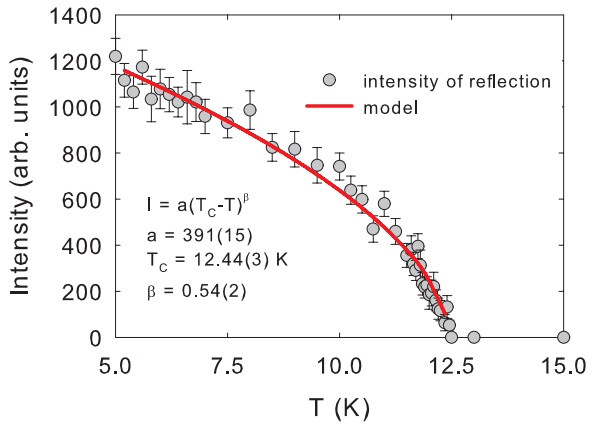

FIG. 9. (Color online) Fit of the intensity of the reflection (5/3, 5/3, 0) as function of temperature.

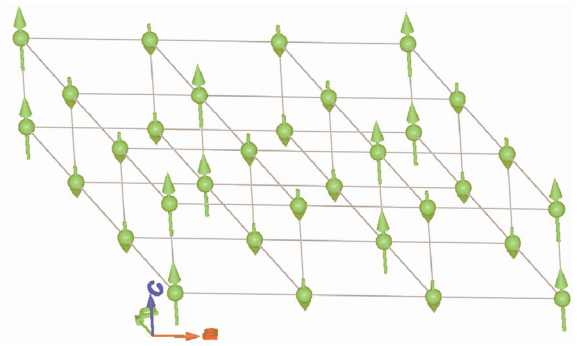

FIG. 10. (Color online) Likely magnetic structure of the phase stable between T_C and T_1 in $SmPd_2Al_3$.

in the scenario of magnetic frustration. As the model example, the isostructural compound $GdPd_2Al_3$ can be considered being presented as a magnetically frustrated Heisenberg triangular lattice antiferromagnet with weak Ising anisotropy.[16,29,30] This can be a key for understanding the magnetic structures of the phases in the phase diagram of the related $SmPd_2Al_3$. Both compounds, $GdPd_2Al_3$ and $SmPd_2Al_3$, have many similarities but also some different magnetic features. The main difference between the Sm and Gd compounds comes from the magnetic state and influence of the crystal field on magnetic ions. The Gd^{3+} ion represents an exception among R ions because of its zero angular momentum. Due to this fact, the multiplet $J = {}^8S_{7/2}$ ground state remains fully degenerated in the crystal field. In the absence of external magnetic field, only an exchange magnetic field can lift the $(2J + 1)$-fold degeneracy.[31,32] The Sm^{3+} ion represents a totally different case as it was suggested in the Introduction. The connecting point between the two compounds is the same hexagonal crystal structure and magnetic $\mathbf{k}$ vector (1/3, 1/3, 0; temperature interval $T_C - T_1$) for $SmPd_2Al_3$ and also for $GdPd_2Al_3$ between T_{N1} and T_{N2}.[16]

Generally, the presence of magnetic frustration in solids is revealed by a few experimental evidences in first simple approach. The first of them is the existence of plateaus in magnetization curves[33–35] and anomalously low θ_{CW} with respect to critical temperatures.[36,37] The empirical quantity $f = -\theta_{CW}/T_C > 1$ (frustration index) corresponds to frustration in most general approach. The investigation of both parameters is pretty complicated for the Sm^{3+} magnetic state. The magnetic susceptibility χ of $SmPd_2Al_3$ is affected by a temperature-independent Van Vleck contribution due to the low-lying first excited multiplet $J = 7/2$ being populated[13] and does not follow the Curie-Weiss law. Despite this fact, the fitted $\theta_{CW} = -21.3$ K using a modified Curie-Weiss law,[1] and found $T_C = 12.5$ K gives $f = 1.7$. Although the frustration index is higher than 1, the generally accepted value for strongly frustrated systems is $f > 10$.[37] In the intermetallic $SmPd_2Al_3$ however, we have to consider the long-range magnetic exchange interactions mediated by conduction electrons contrary to magnetic insulators. In intermetallics then the obtained paramagnetic Curie-Weiss temperature θ_{CW} is proportional to $J(q) = -(J_{ij} * \exp(iq * (r_i - r_j)))$, which may lead to very reduced value of f. Actually, TbNiAl (Ref. 38) and TbPdAl (Ref. 39) are typical Ising-type frustrated magnets; however, their Néel temperature is larger than their θ_p.[40,41] This means the f value is even less than one. We have also analyzed

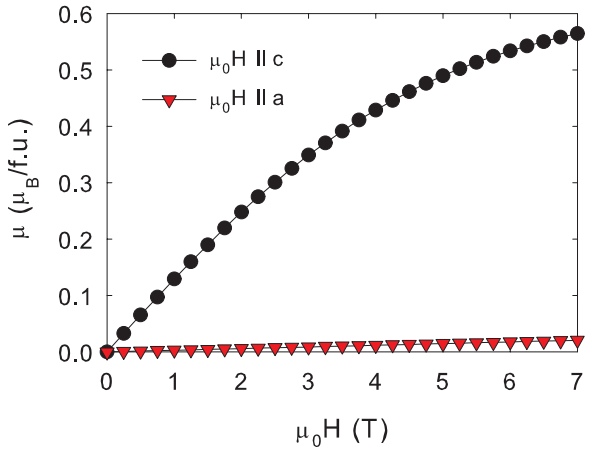

FIG. 11. (Color online) Magnetization isotherms calculated using a crystal field model.

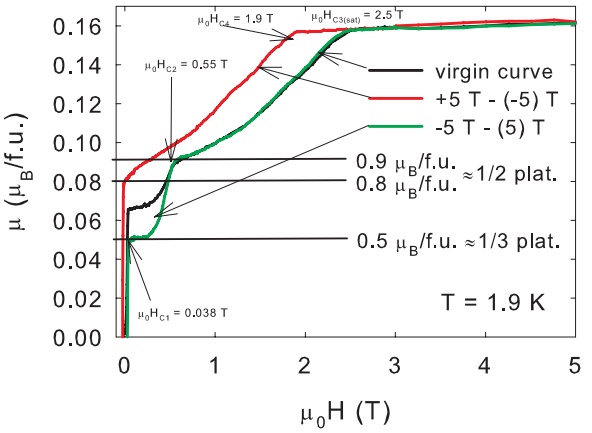

FIG. 12. (Color online) First quadrant of the magnetization loop of $SmPd_2Al_3$ measured at temperature 1.9 K.

the f factor of the generally accepted magnetically frustrated $GdPd_2Al_3$, which is the counterpart of our $SmPd_2Al_3$ system. The value of $f = 2$ was found for $GdPd_2Al_3$,[42] which is in good agreement with $SmPd_2Al_3$ where $f = 1.7$. So, the empirical quantity f does not give a very reasonable result either for $GdPd_2Al_3$ or $SmPd_2Al_3$ to reveal the degree of magnetic frustration.

The analysis of the magnetization plateaus is not straightforward due to the missing knowledge of the saturated moment of the Sm^{3+} ion. For comparison, the isostructural compound $GdPd_2Al_3$ is characterized by the well-defined wide 1/3 plateau on the magnetization curve in the magnetic field interval between 6.2 and 11.8 T.[29,30] Such behavior is typical for triangular lattice antiferromagnets with weak Ising-like anisotropy.

The saturated magnetization value of 0.16 μ_B/f.u. deduced from the magnetization data is significantly less than the expected magnetic moment of $gJ\mu_B = 0.71\,\mu_B$ for the Sm^{3+} free ion. This 0.16 μ_B/f.u. value of the saturated magnetic moment is comparable with value found in Ref. 13. This considerably reduced saturated magnetic moment value by a factor of about five motivated us to carry out the high magnetic field experiment up to 60 T in the pulsed field magnet. The field was applied along the easy-magnetization c axis. The high magnetic field experiment up to 60 T did not show any additional features compared to our lower magnetic field measurement. Especially, the extra magnetic-field induced phases were not observed either along the c axis or in the basal plane.

To gain more insight into our system, we have carried out theoretical calculations. To calculate the magnetic isotherms, we have employed a crystal field model. The microscopic crystal field Hamiltonian has the hexagonal symmetry, and reasonable crystal field parameters were found by first-principles calculations in our previous work.[13] The total (CF + Zeeman) Hamiltonian has been diagonalized, and the obtained eigenvalues and eigenvectors have been used to calculate magnetic isotherms along the axes c and a, respectively. The result of the calculation is presented in Fig. 11.

First, the calculation confirms the c axis as the easy-magnetization axis, but the evolution of the saturated moment is not in reasonable agreement with the experimental data when significantly higher moment has been found—almost three times higher than experimental result in the magnetic field of 5 T. Based on our model, the theoretical field required to reach the saturated magnetic moment is 220 T. However, such a magnetic field is not routinely available now. On the basis of these calculations and experimentally available magnetization data, we still cannot exclude any additional field induced transition in magnetic fields higher than 60 T and the question regarding the value of the saturated magnetic moment is still open.

Presently, we adopt 0.16 μ_B/f.u. as the saturated value (Fig. 12). Then, we find, in the field-increasing process, a plateau around 1/3 of the saturated magnetization and a step to another plateau around 1/2 of the saturated magnetization. The magnetization gradually increases to the saturated magnetization. On the other hand, in the field-decreasing process, the magnetization decreases to 1/2 of the saturated magnetization. Around zero magnetic field, the magnetization shows a sharp change (almost step) to the opposite sign. This feature shows a small hysteresis of $\mu_0 H \approx 0.01$ T. The 1/3 plateau reminds us the magnetization process of antiferromagnets in the triangular (hexagonal) systems. We may also regard the plateau of 0.16 μ_B as the 1/3 plateau, and then we expect another step to the saturated magnetization at higher field. However, the 1/2 plateau does not fit to this picture. Therefore, we cannot take this scenario. Some intermediate kinetic effects could cause the 1/2 plateau in hexagonal systems.[43] Here, a similar kinetic effect is expected for the ordered state. This type of plateau in the increasing field process has been discussed as the magnetic Foehn effect.[44]

According to the simple triangular scenario of XXZ antiferromagnetic model on the hexagonal lattice, the magnetization at $\mu_0 H$ is given by Ref. 33.

$$H_A = \sum_{\langle ij \rangle} \left\{ J\left(S_i^X S_j^X + S_i^y S_j^y\right) + J_z S_i^z S_j^z \right\} - H_z \sum_z S_i^z.$$

The magnetic field at the beginning of the 1/3 plateau is $\mu_0 H_{C1} = 3J$, and the end of the 1/3 plateau is

$$H_{C2} = 3J \frac{(2A - 1 + \sqrt{4A^2 + 4A - 7})}{2}.$$

With $A = J_z/J$. The magnetization at $\mu_0 H = 0$ T is given by

$$M_0 = \frac{(A-1)}{(A+1)}.$$

From the observation, we find $M_0 \cong 1/2$. Thus, we estimate $A \cong 3$. From the value of $\mu_0 H_{C1}$ in the experiment, we estimate $J = 2\mathrm{T}/3$. From these values, $\mu_0 H_{C2}$ is estimated as

$$H_{C2} = 2\ \mathrm{T}(5+\sqrt{41}) \approx 22\ \mathrm{T}.$$

Thus, we may expect another step around $\mu_0 H = 22$ T, but we did not find this step in Fig. 2.

Now, we consider the shape of the magnetization loop from the view point of the kinetic effect. As we saw in the previous section, the magnetization curve of the $SmPd_2Al_3$ at temperature $T = 1.9$ K is characterized by two types of steps (Fig. 12). The first one appears as a step to a plateau of 1/3 of the saturated moment at small value of the magnetic field. The plateau exists in the magnetic field interval $\mu_0 H_{C1} = 0.04$ T and $\mu_0 H = 0.25$ T. Next, the magnetization increases and reaches 1/2 of saturated moment to full saturated value at $\mu_0 H_{C2} = 0.55$ T. Then, the magnetization curve has a kink or a small plateau, and the magnetization gradually increases to the full saturated value. It reaches the saturated moment at $\mu_0 H_{C3} = 2.5$ T. In the process of decreasing magnetic field, the magnetization begins to decrease from the saturated value at $\mu_0 H_{C4} = 1.9$ T and decreases gradually to near 1/2 of saturated moment and step to the negative value. Because of the hysteresis of the magnetization process, the magnetization curve cannot be considered in truth as a plateau.

It is also necessary to consider other effects that can lead to the induction of the plateaus and jumps in on magnetization curves. Dynamical magnetic processes have been found in single molecular magnets and also magnetic rings.[45] For example, a phonon-bottleneck effect in V_{15},[46] which was explained as a phenomenon due to lack of phonon mode for the equilibration. Similar phenomena were observed in $[Fe(salen)Cl]_2$ (Ref. 47) and also Fe_{10}. (Ref. 48) These phenomena can be regarded as adiabatic processes with a small inflow of heat. The influence of the kinetic effect of a sweeping magnetic field is understood as a magnetic Foehn effect.[34,35] A similar phenomenon has been observed in macroscopic magnetization processes. For example, Katsumata *et al.* has found it in $FeCl_2.2H_2O$ (Ref. 43) and also Narumi *et al.* in a Kagome lattice.[49]

In the present case, the step is found in a macroscopic change of magnetization. To clarify the influence of the sweeping magnetic field on magnetization, we have measured magnetization loop both with a slow-field rate in the SQUID magnetometer and in a pulse field magnet, where the maximum used field of 8 T was reached within a few tens of milliseconds. The results are shown in the Fig. 13.

The original 1/3 plateau has been shifted to higher magnetic field (from original field region $\mu H_{C1} = 0.04$ T and $\mu_0 H_{C2} = 0.55$ T to $\mu_0 H_{C1} = 0.35$ T and $\mu_0 H_{C2} = 1.35$ T). In addition, the original 1/3 and 1/2 plateaus have not conserved their characteristic and have been suppressed to the lower and higher magnetic moments, respectively. Even the saturation has been reached at a significantly higher magnetic field of

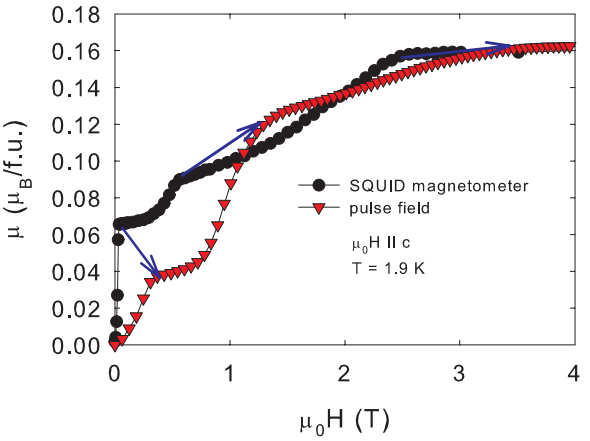

FIG. 13. (Color online) Virgin magnetization curves measured in various magnetic field sweep rates. All steps (plateaus) have been shifted to higher field in the case of pulse field magnetization experiment. The red (full line) arrows mark the shift of the 1/3 plateau. The blue (dashed) arrows mark the shift of the 1/2 step.

$\mu_0 H_{C3} \approx 3.5$ T. We have suggested a scenario of the kinetic effect on the magnetization of $SmPd_2Al_3$. There, we find large change of the magnetization process where even the height of the plateau changes. Thus, we have to consider that the ordered state has a rather complicated structure and various metastable states exist. In general, a plateau indicates a collinear structure (e.g., up-up-down structure), while gradual increase indicates a noncollinear structure (e.g., the Y-shape structure). In Figs. 3–5, we found that the temperature simply smears the structure, but in Fig. 13, the spin structure at intermediate magnetic field seems to be different in the SQUID measurement and the pulse field measurement. Unfortunately, at this moment, we cannot identify the structure with the data available now. Further detailed observations are expected.

VII. CONCLUSIONS

Within the $SmPd_2Al_3$ study, we have established the magnetic phase diagram on the basis of magnetization data. We have found a rather complicated magnetic phase diagram, where five different magnetic phases appear with pronounced hysteresis of two phases. We have detected a rather reduced saturated magnetic moment (0.16 μ_B/f.u.) for Sm^{3+} ion that is most probably given by a strong crystal field effect. Even applying a high magnetic field of 60 T has not led to any significant increase of the saturated magnetization. Although, the constructed magnetic phase diagram brings considerable progress in knowledge of the Sm magnetism in $SmPd_2Al_3$ compound, detailed information regarding their magnetic structures has still been lacking.

Therefore, we have performed a neutron diffraction experiment of $SmPd_2Al_3$ single crystal, and we have successfully observed magnetic reflection (5/3, 5/3, 0) and its equivalents in the temperature interval 12.4–4.4 K, which denotes the magnetic **k** vector (1/3, 1/3, 0). Consequently, $SmPd_2Al_3$ material can be considered as belonging to the group of magnetically frustrated systems. Based on our observations, we expect a triangular lattice antiferromagnet with weak

Ising-like anisotropy as the most suitable model for $SmPd_2Al_3$ compound.

The pulsed high magnetic field magnetization experiment surprisingly points to the influence of kinetic effect in magnetization process. The kinetic effect turns out to be the partially responsible effect for steplike shape of magnetization curves at low temperatures, where various rates of external field sweep lead to different metastable magnetic states.

On the basis of our investigation, the $SmPd_2Al_3$ compound represents a unique example of a complicated three-dimensional (3D) phase diagram when not only the temperature and magnetic field are external variables but also the field sweep rate plays an important role. The rich magnetic phase diagram is given by a unique interplay of the magnetic frustration with kinetic effect of the sweeping magnetic field.

Although many features of the Sm magnetism in $SmPd_2Al_3$ have been conceived, some questions regarding the magnetic structures of the low-temperature phases remain unresolved. In particular, the question of the existence of the off *c* axis component of the magnetic moment seems to be most essential. Magnetic x-ray resonant scattering performed on Sm absorption edge, polarized neutron diffraction, and fine measurements on torque magnetometer may reveal be helpful.

ACKNOWLEDGMENTS

This work was supported by the Czech Science Foundation (GACR P204/12/0692). Experiments performed in the Magnetism and Low Temperature Laboratories at Charles University in Prague were supported within the program of Czech Research Infrastructures (Project No. LM2011025). Neutron diffraction experiments in ILL, Grenoble, were performed within Project No. LG11024, financed by the Ministry of Education of the Czech Republic. High-field magnetization measurements were supported by EuroMagNET under the EU Contract No. 228043.

[1] A. Dönni, A. Furrer, H. Kitazawa, and M. Zolliker, J. Phys.: Condens. Matter **9**, 5921 (1997).
[2] A. Dönni, A. Furrer, E. Bauer, H. Kitazawa, and M. Zolliker, Z. Phys. B **104**, 403 (1997).
[3] A. Dönni, H. Kitazawa, P. Fischer, T. Vogt, A. Matsushita, Y. Iimura, and M. Zolliker, J. Solid State Chem. **127**, 169 (1996).
[4] K. Ghosh, S. Ramakrishnan, A. D. Chinchure, V. R. Marathe, and G. Chandra, Physica B **223-224**, 354 (1996).
[5] K. Ghosh, S. Ramakrishnan, S. K. Malik, and G. Chandra, Phys. Rev. B **48**, 6249 (1993).
[6] K. Ghosh, S. Ramakrishnan, S. K. Malik, and G. Chandra, Physica B **199-200**, 604 (1994).
[7] H. Kitazawa, A. Mori, S. Takano, T. Yamadaya, A. Matsushita, and T. Matsumoto, Physica B **188**, 661 (1993).
[8] G. Motoyama, T. Nishioka, and N. K. Sato, J. Phys. Soc. Jpn. **71**, 1609 (2002).
[9] S. A. M. Mentink, N. M. Bos, G. J. Nieuwenhuys, A. A. Menovsky, and J. A. Mydosh, Physica B **186–188**, 497 (1993).
[10] J. Pospisil, M. Kratochvilova, M. Divis, J. Prokleska, J. Vejpravova Poltierova, and V. Sechovsky, J. Alloys Compd. **509**, 1401 (2011).
[11] A. M. Strydom and P. de V. Du Plessis, J. Magn. Magn. Mater. **226–230**, 150 (2001).
[12] V. S. Zapf, R. P. Dickey, E. J. Freeman, C. Sirvent, and M. B. Maple, Phys. Rev. B **65**, 024437 (2001).
[13] J. Pospisil, M. Kratochvilova, J. Prokleska, M. Divis, and V. Sechovsky, Phys. Rev. B **81**, 024413 (2010).
[14] Z. S. Liu, Physica B **262**, 348 (1999).
[15] Z. S. Liu, Phys. Rev. B **64**, 144407 (2001).
[16] T. Inami, N. Terada, H. Kitazawa, and O. Sakai, J. Phys. Soc. Jpn. **78**, 084713 (2009).
[17] G. H. Dieke, *Spectra and Energy Levels of Rare Earth Ions in Crystals* (John Wiley & Sons, New York, 1968).
[18] H. W. Dewijn, A. M. Vandiepe, and K. H. J. Buschow, Phys. Rev. **161**, 253 (1967).
[19] J. K. Böhlke, J. R. d. Leater, P. D. Bièvre, H. Hidaka, H. S. Peisar, K. J. R. Rosman, and P. D. P. Taylor, J. Phys. Chem. Ref. Data **34**, 57 (2005).
[20] K. J. R. Rosman and P. D. P. Taylor, Pure Appl. Chem. **70**, 217 (1998).
[21] F. V. Sears, Neutron News **3**, 26 (1992).
[22] A. J. Dempster, Phys. Rev. **74**, 505 (1948).
[23] R. E. Lapp, J. R. Vanhorn, and A. J. Dempster, Phys. Rev. **71**, 745 (1947).
[24] Nuclear Date Services, http://www-nds.iaea.org/ngatlas2/.
[25] K. A. Toukan, K. Debus, F. Kappeler, and G. Reffo, Phys. Rev. C **51**, 1540 (1995).
[26] K. Wisshak, K. Guber, F. Voss, F. Kappeler, and G. Reffo, Phys. Rev. C **48**, 1401 (1993).
[27] M. S. Lehmann, W. Kuhs, G. J. McIntyre, C. Wilkinson, and J. Allibon, J. Appl. Crystallogr. **22**, 562 (1989).
[28] C. Wilkinson, H. W. Khamis, R. F. D. Stansfield, and G. J. McIntyre, J. Appl. Crystallogr. **21**, 471 (1988).
[29] H. Kitazawa, H. Suzuki, H. Abe, J. Tang, and G. Kido, Physica B **259–261**, 890 (1999).
[30] H. Kitazawa, K. Hashi, H. Abe, N. Tsujii, and G. Kido, Physica B **294-295**, 221 (2001).
[31] K. H. J. Buschow and F. R. de Boer, *Physics of Magnetism and Magnetic Materials* (Kluwer Academic, New York, 2003).
[32] M. Bouvier, P. Lethuillier, and D. Schmitt, Phys. Rev. B **43**, 13137 (1991).
[33] S. Miyashita, J. Phys. Soc. Jpn. **55**, 3605 (1986).
[34] K. Penc, N. Shannon, and H. Shiba, Phys. Rev. Lett. **93**, 197203 (2004).
[35] H. Nishimori and S. Miyashita, J. Phys. Soc. Jpn. **55**, 4448 (1986).
[36] C. Lacroix, P. Mendels, and F. Mila, *Introduction to Frustrated Magnetism: Materials, Experiments, Theory* (Springer-Verlag, Berlin, 2011).
[37] A. P. Ramirez, Annu. Rev. Mater. Sci. **24**, 453 (1994).
[38] G. Ehlers, C. Ritter, J. R. Stewart, A. D. Hillier, and H. Maletta, Phys. Rev. B **75**, 024420 (2007).
[39] A. Donni, L. Keller, H. Kitazawa, J. Prchal, and P. Fischer, J. Alloys Compd. **464**, 67 (2008).
[40] H. Kitazawa, S. Eguchi, and G. Kido, Physica B **359**, 223 (2005).
[41] H. Kitazawa, S. Eguchi, and G. Kido, Physica B **329**, 1053 (2003).
[42] H. Kitazawa (private communication).
[43] K. Katsumata, J. Phys. Soc. Jpn. **39**, 42 (1975).

[44]K. Saito and S. Miyashita, J. Phys. Soc. Jpn. **70**, 3385 (2001).
[45]E. C. Yang, W. Wernsdorfer, L. N. Zakharov, Y. Karaki, A. Yamaguchi, R. M. Isidro, G.-D. Lu, S. A. Wilson, A. L. Rheingold, H. Ishimoto, and D. N. Hendrickson, Inorg. Chem. **45**, 529 (2006).
[46]I. Chiorescu, W. Wernsdorfer, A. Muller, H. Bogge, and B. Barbara, Phys. Rev. Lett. **84**, 3454 (2000).
[47]Y. Shapira, M. T. Liu, S. Foner, C. E. Dube, and P. J. Bonitatebus, Phys. Rev. B **59**, 1046 (1999).
[48]H. Nakano and S. Miyashita, J. Phys. Soc. Jpn. **70**, 2151 (2001).
[49]Y. Narumi, K. Katsumata, Z. Honda, J. C. Domenge, P. Sindzingre, C. Lhuillier, Y. Shimaoka, T. C. Kobayashi, and K. Kindo, Europhys. Lett. **65**, 705 (2004).